

Hybrid Conformal Prediction-based Risk-Aware Model Predictive Planning in Dense, Uncertain Environments

Jeongyong Yang^{1*}, KwangBin Lee^{1*}, and SooJean Han¹

Abstract—Real-time path planning in dense, uncertain environments remains a challenging problem, as predicting the future motions of numerous dynamic obstacles is computationally burdensome and unrealistic. To address this, we introduce Hybrid Prediction-based Risk-Aware Planning (HyPRAP), a prediction-based risk-aware path-planning framework which uses a hybrid combination of models to predict local obstacle movement. HyPRAP uses a novel Prediction-based Collision Risk Index (P-CRI) to evaluate the risk posed by each obstacle, enabling the selective use of predictors based on whether the agent prioritizes high predictive accuracy or low computational prediction overhead. This selective routing enables the agent to focus on high-risk obstacles while ignoring or simplifying low-risk ones, making it suitable for environments with a large number of obstacles. Moreover, HyPRAP incorporates uncertainty quantification through *hybrid conformal prediction* by deriving confidence bounds simultaneously achieved by multiple predictions across different models. Theoretical analysis demonstrates that HyPRAP effectively balances *safety* and *computational efficiency* by leveraging the diversity of prediction models. Extensive simulations validate these insights for more general settings, confirming that HyPRAP performs better compared to single predictor methods, and P-CRI performs better over naive proximity-based risk assessment.

I. INTRODUCTION

Real-time planning in stochastic environments with dynamic obstacles remains a challenging problem, particularly in crowded scenarios such as pedestrian-dense streets or industrial warehouses. Kinodynamic motion planning methods [1–3], including *model predictive control* (MPC), have been especially popular to use as modern path-planning techniques due to their ability to integrate multiple constraints (e.g., collision-avoidance, agent dynamics). More importantly, optimization-based control approaches like MPC [4, 5] provide a natural way to incorporate *motion predictions* making it especially suitable for real-time control.

A recent body of work on MPC path-planning using predictions of *obstacle* motion has been focused on ensuring *safety guarantees* in collision-avoidance conditions by quantifying the uncertainty of the moving obstacles via *conformal prediction* (e.g., [6, 7]). However, many of these existing approaches rely on generating predictions and quantifying uncertainty for nearly *all* of the obstacles present in the environment. For densely populated environments where the number of obstacles is very large, this can make real-time execution computationally burdensome, if not infeasible. Several studies have been introduced to reduce the

computational complexity of prediction while maintaining a reasonably high accuracy [8, 9]. But it is still inefficient to generate predictions for all obstacles to the same degree of accuracy and computational energy, due to the agent’s nonuniform interaction with the obstacles as they move in the environment over time. Moreover, high-accuracy predictions generally require more inference time, a consequence of the fundamental *accuracy-efficiency tradeoff* prevalent in prediction problems and more [10]. Meanwhile, in the collision-avoidance literature, metrics such as *collision risk index* (CRI) [11] have been introduced as a way to estimate how likely collisions are to occur, and have been widely used in many path-planning applications. These metrics provide a natural way to determine how to prioritize prediction resources based on which obstacles are of the highest risk to the agent.

This paper proposes a motion planning framework that integrates *hybrid prediction* into optimization-based path-planning, with safety guarantees achieved through uncertainty quantification. Our main development is the hybrid prediction model, which is essentially a collection of (at least) two prediction models, including computationally heavy but accurate predictors and lighter but comparably inaccurate predictors. The approach is inspired by the System 1-System 2 thinking process of the human brain [12] and subsequent application in the engineering community (e.g., [13, 14]), which have demonstrated that combining a diversity of model specifications enables the achievement of a more optimal balance between high accuracy and fast efficiency compared to methods that use only one model. Furthermore, we introduce a *Prediction-based Collision Risk Index* (P-CRI) method which dynamically routes each locally-sensed obstacle to a corresponding predictor based on a novel risk index of our design. This allows the agent to prioritize the most safety-critical obstacles at the best possible attainment of accuracy and efficiency, making real-time motion planning feasible even in highly dynamic and dense environments.

II. RELATED WORK

A. Uncertainty-Aware Real-Time Planning

MPC has been widely used as a robust and effective framework for real-time path planning, due to its ability to handle numerous feasibility constraints, including static obstacles and the predicted motions of dynamic obstacles [15, 16]. However, increasing the amount of prediction done per obstacle also increases the number of constraints in the MPC problem, and so its computational complexity makes

*Both authors contributed equally to this work.

¹School of Electrical Engineering, Korea Advanced Institute of Science and Technology (KAIST), Daejeon 34141, Republic of Korea. Correspondence to: seiryu2238@kaist.ac.kr

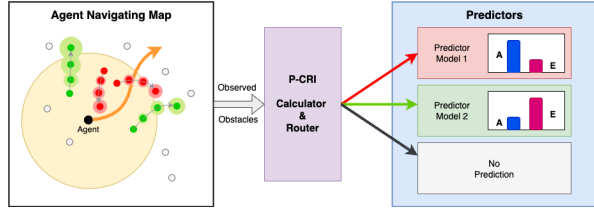


Fig. 1: Overall HyPRAP architecture. [Left] A sample environment with the agent (black dot) and the dynamic obstacles. Predicted paths of each obstacle (red/green) have corresponding uncertainty regions (shaded). Obstacles within sensing range (yellow) have their risks assessed (purple box). [Right] Each obstacle is routed to an appropriate trajectory predictor (blue box); obstacles can be excluded from prediction (gray) if it is deemed low risk.

the MPC solver more likely to be infeasible [17]. To mitigate this, probabilistic methods such as chance-constrained MPC [18, 19] were introduced as a means to incorporate obstacle uncertainty more softly into planning, but many of these approaches assume predefined uncertainty distributions. Conformal prediction [20, 21] offers a distribution-free alternative to uncertainty quantification with finite-sample safety guarantees, and provides a neat integration into the MPC framework via calibrated confidence bounds [6, 7]. On the model-free side, Bayesian inference [22, 23] has also been used to provide probabilistic guarantees in trajectory predictions, making them valuable for more robust and risk-aware navigation.

B. Prediction Models for Obstacle Motion

Crucial to real-time safe navigation in our approach is fast and efficient obstacle motion prediction and inference, for which many such methods have been proposed. Traditional model-based predictors like the Kalman filter family [24, 25], particle filters [26, 27], and hidden Markov models [28, 29] are still widely used for tracking and forecasting obstacle motion in the present day. Recent advances in big data and compute have made it possible to construct increasingly complex models for predicting highly uncertain behaviors, e.g., pedestrian movement. To this end, data-driven approaches to trajectory prediction, such as Long Short-Term Memory (LSTM) networks [30, 31] and Gaussian Process Regression (GPR) [32], have also emerged.

C. Assessing the Risk of Collisions

Collision risk index (CRI) has been widely used in maritime navigation [11, 33] to quantify potential collision risks. CRI was generally measured using the closest point of approach (CPA) metric [34], and other common extensions of CPA include distance at the CPA (DCPA) and time to CPA (TCPA) [35]. Although these measures are largely effective in deterministic scenarios, they do not consider the uncertainty of predicted trajectories for obstacles over time.

III. PROBLEM FORMULATION

We consider scenarios in which a single agent must navigate towards a designated goal within a dynamic environment. The agent abides by some general discrete-time dynamics $\mathbf{x}_{t+1} = f(\mathbf{x}_t, \mathbf{u}_t)$ at each time $t \in \mathbb{Z}^{\geq 0}$, with state $\mathbf{x}_t \in \mathbb{R}^n$ and control input $\mathbf{u}_t \in \mathbb{R}^m$. A static map of the

environment and the position of the goal are known to the agent at initial time. The agent has sensors that let it observe any local changes in its sensing range.

The environment is dynamic in that it contains a set $\mathcal{N} \triangleq \{1, \dots, N\}$ ($N \in \mathbb{N}$) of moving obstacles, each of which travels according to its own dynamics unknown to the agent. While our method can be used in environments containing a mixture of static and dynamic obstacles, we currently remove static obstacles to keep our discussion focused. We define $\mathcal{N}_t \subseteq \mathcal{N}$ ($N_t \triangleq |\mathcal{N}_t|$) to be the subset (number) of obstacles within the agent's sensing range at each time t . As state estimation is not the main focus of our paper, we assume there is no sensor noise, i.e., the position of each obstacle in sensing range can be exactly measured.

IV. SAFE PLANNING WITH HYBRID PREDICTION

A. Key Ideas and Notations of HyPRAP

To safely reach its goal in the environment, our agent uses the *closed-loop model predictive control (MPC)* framework to generate control policies in real time. To better distribute the limited time and computational resources of the agent, we equip it with a collection \mathcal{P} of multiple predictors with different performance specifications. Details in Section IV-C.

Because creating accurate predictions for *all* local obstacles is computationally burdensome, our agent assesses which ones have the highest risk (e.g., pedestrians further away from an autonomous car have less collision risk). This is our *first key idea*: we design a novel collision-risk metric ψ and routing function ϕ to assign an appropriate prediction model $P^{\phi(t,k)} \in \mathcal{P}$ to each obstacle $k \in \mathcal{N}_t$. Details are in Section IV-D. We further designate obstacles with very low ψ (risk) as *insignificant* to safe motion planning, and exclude it from prediction. We define $\mathcal{M}_t \subseteq \mathcal{N}_t$ ($|\mathcal{M}_t| = M_t$) to be the set (number) of obstacles to be predicted at time t .

Our *second key idea* comes from the diversity of predictors \mathcal{P} . Once $P^{\phi(t,k)}$ is decided, the predicted future trajectory $\hat{Y}_k^{\phi(t,k)}[\cdot|t] \triangleq [\hat{Y}_k^{\phi(t,k)}[t+1|t], \dots, \hat{Y}_k^{\phi(t,k)}[t+H|t]] = P^{\phi(t,k)}(Y_k[t]; \delta, H)$ is generated by taking $Y_k[t]$, obstacle k 's current position at time t , as input. Here, $Y_k[t]$ is fully known if $k \in \mathcal{N}_t$, and $\hat{Y}_k^{\phi(t,k)}[t+h|t] \in \mathbb{R}^n$ represents the predicted states of obstacle k under predictor $P^{\phi(t,k)}$ at future time $t+h$ after the current time t , where $h \in \{1, \dots, H\}$. User-chosen parameters are the *prediction horizon* $H \in \mathbb{N}$ and the *failure rate* $\delta \in (0, 1)$, which corresponds to a *confidence level* $1 - \delta$. Details are in Section IV-B.

B. Hybrid Conformal Prediction

Many standard conformal prediction-based planning methods in the literature construct uncertainty regions based off only one predictor. To support the second key idea (see Section IV-A) of our controller architecture, we developed *hybrid conformal prediction*, a multi-predictor version of conformal prediction which computes uncertainty bounds for multiple prediction models.

For each single obstacle $k \in \mathcal{N}_t$ at time t using prediction model $P^{\phi(t,k)} \in \mathcal{P}$, we want to ensure

$$\mathbb{P}(\|Y_k[t+h] - \hat{Y}_k^{\phi(t,k)}[t+h|t]\| \leq \epsilon^{\phi(t,k)}[t+h|t]) \geq 1 - \delta \quad (1)$$

where $h \in \{1, \dots, H\}$. Essentially, (1) ensures that the error between the true and predicted future positions of obstacle k remains inside the ball of conformal radius $\epsilon^{\phi(t,k)}[t+h|t] \in \mathbb{R}^+$ with sufficiently high probability. Here “sufficiently high” is determined by user-chosen confidence level $1 - \delta$, and $\epsilon^{\phi(t,k)}[t+h|t]$ is calculated using pre-collected calibration data for $P^{\phi(t,k)}$, as explained in [6].

The condition (1) is extended to apply for the entire prediction horizon with a choice of quantile $\bar{\delta} \triangleq \delta/H$ in (1) (see Lemma 1 of [6]):

$$\mathbb{P}(\|Y_k[t+h] - \hat{Y}_k^\ell[t+h|t]\| \leq \epsilon^\ell[t+h|t], \forall h \in \{1, \dots, H\}) \geq 1 - \delta, \quad \text{with placeholder } \ell \triangleq \phi(t, k) \quad (2)$$

We assume each predictor operates independently of each other (i.e., the result of one predictor is not used in any other predictor); relaxing this assumption is future work.

Remark 1. With local sensing and distinct prediction models per obstacle, it becomes important to emphasize the dependence of δ on M_t , unlike prior works (e.g. [6, 7]) which set δ for the entire set of obstacles \mathcal{N} . We also assign δ based on the predictor used for each obstacle, as in (1), rather than applying it to the stacked vector of all obstacles, as done in [6, 7]. This allows the confidence levels to naturally reflect both the heterogeneity of the predictors and the changing M_t .

C. Model Predictive Control for Safe Planning

To generate control inputs, we use closed loop MPC with collision avoidance constraints based on obstacle trajectory predictions $\hat{Y}^{\phi(t,k)}[:, t]$.

$$\min_{\mathbf{u}_{t:t+T-1}} J(\mathbf{x}, \mathbf{u}) \triangleq \sum_{\tau=0}^{T-1} \mathcal{L}(\mathbf{x}_{t+\tau}, \mathbf{u}_{t+\tau}) + \mathcal{L}_f(\mathbf{x}_{t+T}) \quad (3a)$$

$$\text{s.t. } \mathbf{x}_{t+\tau+1} = f(\mathbf{x}_{t+\tau}, \mathbf{u}_{t+\tau}) \quad (3b)$$

$$\mathbf{u}_{t+\tau} \in \mathcal{U}, \quad \mathbf{x}_{t+\tau+1} \in \mathcal{X} \quad (3c)$$

$$c(\mathbf{x}_{t+h}, \hat{Y}_k^{\phi(t,k)}[t+h|t]) \geq L\epsilon^{\phi(t,k)}[t+h|t] \quad (3d) \\ \forall \tau \in \{0, \dots, T-1\}, h \in \{1, \dots, H\}, k \in \mathcal{M}_t$$

where \mathcal{L} and \mathcal{L}_f are respectively the running and terminal costs, \mathcal{X} and \mathcal{U} are convex sets, and T is the *planning horizon* for solving the MPC problem. We incorporate the conformal regions from Section IV-B into the control problem via (3d), with c being the convex collision-avoidance constraint with Lipschitz constant L , following the notation of [6]. In order for (3) to be well-posed, the user must choose $H \leq T$; one natural choice is $T = H$.

Together with (2), note that the property of recursive feasibility is satisfied in a way similar to Theorem 3 of [6]. That is, if at time t , the optimization problem (3) is feasible with planning horizon T , the control sequence satisfies

$$\mathbb{P}(c(\mathbf{x}_{t+\tau}, Y[t+\tau]) \geq 0, \forall \tau \in \{1, \dots, T\}) \geq 1 - \delta \quad (4)$$

One difference here is that due to using multiple prediction models, there are two cases that could occur for each obstacle k . The first case is that $\phi(t, k) = \phi(t+1, k)$ (i.e., the same model ℓ is used to generate consecutive predictions $\hat{Y}^\ell[:, t]$

and $\hat{Y}^\ell[:, t+1]$), and the second case is that $\phi(t, k) \neq \phi(t+1, k)$. However, because each predictor $P^\ell \in \mathcal{P}$ satisfies (2) and each predictor operates independently of each other, feasibility is inductively (recursively) satisfied.

One important subcase of the second case is when $k \in \mathcal{N}_t \setminus \mathcal{M}_t$ and $k \in \mathcal{M}_{t+1}$, because $\phi(t, k)$ may be ill-defined for $k \in \mathcal{N}_t \setminus \mathcal{M}_t$. We discuss this further in the next Section IV-D, where we concretely define ϕ (and ψ).

D. Prediction-based Collision Risk Index

To support the first key idea of Section IV-A, each obstacle is routed to the appropriate predictor based on how much of a risk it poses to the agent. We propose the novel *Prediction-based Collision Risk Index (P-CRI)*, which quantifies collision risk by incorporating the predicted trajectories of both the agent and obstacles.

Measuring Risk of All Local Obstacles. We define the *prediction-based approach distances* (PAD) and *prediction-based approach times* (PAT) for each obstacle k as follows:

$$\text{PAD}(t, k) = [\|\mathbf{p}_A(t+h) - \mathbf{p}_k(t+h)\|]_{h=0}^H \quad (5a)$$

$$\text{PAT}(t, k) = \quad (5b)$$

$$\left[\frac{(\mathbf{p}_k(t+h) - \mathbf{p}_A(t+h))^\top (\mathbf{v}_A(t+h) - \mathbf{v}_k(t+h))}{\|\mathbf{v}_A(t+h) - \mathbf{v}_k(t+h)\|^2} \right]_{h=0}^H$$

where for each $h \in \{0, \dots, H\}$, $\mathbf{p}_A(t+h)$ and $\mathbf{p}_k(t+h)$ are the predicted position vectors of the agent and obstacle k , respectively. The agent's predicted position $\mathbf{p}_A(t+h)$ can be extracted from \mathbf{x}_{t+h} (from (3)), and obstacle k 's predicted position $\mathbf{p}_k(h)$ from $\hat{Y}[t+h|t]$ ($Y[t]$ if $h=0$). The \mathbf{v} represents the velocity vectors, obtained via backward difference of the position vectors. Essentially, $\text{PAD}(t, k) \in \mathbb{R}_{\geq 0}^{H+1}$ captures the distance between the obstacle and the agent over the entire prediction horizon, while $\text{PAT}(t, k) \in \mathbb{R}^{H+1}$ captures the projection of the relative position vector onto the relative velocity vector, effectively indicating how aligned the predicted obstacle is with the agent's direction of motion. Note that $h=0$ includes the current time t , unlike the prediction horizon h from (3) which starts from time $t+1$.

The P-CRI ψ for each obstacle k is now obtained by combining PAD and PAT through a weighted average:

$$\psi(t, k) \triangleq w_1 g_1(\text{PAD}(t, k)) + w_2 g_2(\text{PAT}(t, k)) \quad (6)$$

where w_1, w_2, g_1, g_2 are user-chosen weights and functions which balance the collision risk by proximity and temporal urgency. In general, $g_1(x)$ should decrease monotonically, while $g_2(x)$ increases monotonically when $x < 0$ is negative, decreases monotonically when $x > 0$, and continuous at $x=0$, e.g. a double-sided exponential. For convenience, w_1, w_2, g_1, g_2 are chosen so that $\psi(t, k) \in [0, 1]$, $\forall t, k$.

Routing Obstacles to Prediction Models. Each observed obstacle k is routed to a prediction model according to $\phi(\psi(t, k))$, where ϕ is the routing function that assigns each obstacle k to one of the prediction models in \mathcal{P} . For notation simplicity, we will write $\phi(t, k)$ without the ψ throughout the paper. For concreteness, we used a simple

thresholding mechanism to route based on P-CRI: given a partition $\{\theta_0, \theta_1, \dots, \theta_{|\mathcal{P}|}\}$ of thresholds, where $\theta_0 = 0$ and $\theta_{|\mathcal{P}|} = 1$, we choose $\phi(t, k) = \ell$ if $\psi(t, k) \in [\theta_\ell, \theta_{\ell+1})$.

The routing mechanism is intuitive: obstacles that have a higher P-CRI are, by definition, at a higher risk of collision with the agent, and should be predicted at the highest possible accuracy; therefore, they are routed to more accurate predictors (even if they may be computationally intensive). Conversely, lower P-CRI obstacles are routed to less computationally intensive and relatively inaccurate predictors, since they are not as urgent to the agent. The lowest-risk obstacles, i.e., $\phi(t, k) = 0$, are treated the same way as obstacles in $\mathcal{N}_t \setminus \mathcal{M}_t$, and not predicted using any model from \mathcal{P} . But, to make (5) well-defined for the next timestep, we use “simpler” (very low-complexity) predictors, e.g., either stationary or constant-velocity. This additional step makes (3) recursively feasible even as obstacles switch predictors over time. Currently, we do not incorporate obstacle motions from these “simpler” predictors as MPC constraints in (3). HyPRAP is summarized by Algorithm 1.

Algorithm 1 Hybrid Conformal Prediction-based P-CRI Model Predictive Planning

Inputs: Predictors \mathcal{P} , P-CRI router ϕ , planning and prediction horizons T and H , failure rate δ .
Output: Optimal control sequence $\{\mathbf{u}_t\}$

- 1: For $P^\ell \in \mathcal{P}$, compute ϵ^ℓ given δ (Sec. IV-B) # Offline
- 2: Initialize $\mathbf{x}_{0:H}$, \mathbf{u}_0 and $\hat{Y}_k^{\phi(0,k)}$.
- 3: **for** each time step t **do** # Online Planning Loop
- 4: Observe local obstacles $\{Y_k[t] : k \in \mathcal{N}_t\}$.
- 5: Initialize $\mathcal{M}_t \leftarrow \emptyset$.
- 6: **for** each obstacle $k \in \mathcal{N}_t$ **do** ▷ P-CRI
- 7: Update $\phi(t, k)$ by $\mathbf{x}_{t-1:t+H-1}$, $\hat{Y}_k^{\phi(t-1,k)}[t-1]$
- 8: **if** $\phi(t, k) \neq 0$ **then**
- 9: $\mathcal{M}_t \leftarrow \mathcal{M}_t \cup \{k\}$
- 10: **end if**
- 11: **end for**
- 12: **for** each $k \in \mathcal{M}_t$ **do** ▷ Prediction
- 13: $\hat{Y}_k^{\phi(t,k)}[t] \leftarrow P^{\phi(t,k)}(Y_k[t])$
- 14: **end for**
- 15: Solve MPC in (3) to get \mathbf{u}_t and save $\mathbf{x}_{t:t+H}$.
- 16: Apply control input \mathbf{u}_t .
- 17: **end for**

V. THEORETICAL ANALYSIS

It is well-known in both the control systems and neuroscience literature that implementing a system using components that have a diversity of specifications improves overall system performance [12, 14]. We show that the same trends apply to HyPRAP since the diversity of specifications comes from the usage of different prediction models.

A. Setting for the Theory

In this section, we focus on the case with $|\mathcal{P}| = 2$ distinct prediction models and a time t where $M_t = N_t$. For the concreteness of our analysis, we assign some variables to

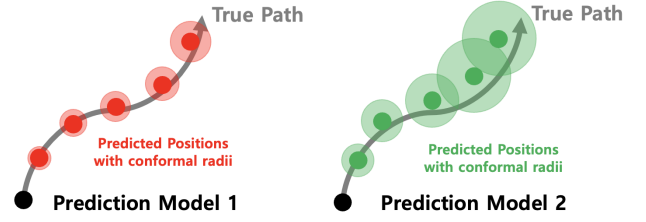


Fig. 2: Sample visualization of P^1 versus P^2 . Since P^1 is more accurate than P^2 , the uncertainty regions (shaded) around each prediction point (solid dot) are smaller compared to those of P^2 .

the individual specifications of each predictor as follows. As before, the conformal radius, $\epsilon^\ell[t + h|t]$ from (1), quantifies the inaccuracy of predictor P^ℓ for each obstacle at fixed confidence level $1 - \delta$. The smaller the conformal radius, the more accurate the predictor. We also assign variable $\Delta T^\ell \propto H$ to be the amount of computation time it takes P^ℓ to compute a future trajectory $\hat{Y}_k^{\phi(t,k)}[t]$ for a single obstacle k at time t . We set P^1 to have higher accuracy and lower computational efficiency (speed) compared to P^2 , i.e., $\epsilon^1 < \epsilon^2$, and $\Delta T^1 > \Delta T^2$.

We are comparing three main prediction architectures, which all employ P-CRI to assess obstacle risks, but differ by prediction model.

- SP¹: (3) uses only predictor P^1 to obtain $\hat{Y}_k^1[|t|]$, i.e., $\phi(t, k) = 1, \forall k \in \mathcal{M}_t$.
- HyPRAP: the original (3) as we proposed, which dynamically selects P^1 or P^2 via P-CRI $\phi(t, k)$.
- SP²: (3) uses only predictor P^2 to obtain $\hat{Y}_k^2[|t|]$, i.e., $\phi(t, k) = 2, \forall k \in \mathcal{M}_t$.

We focus on *efficiency* and *safety* as competing metrics of performance for each architecture in this section.

B. Efficiency Analysis

Lemma 1 (Efficiency of HyPRAP). Under the setting of Section V-A, suppose HyPRAP routes $M^1 (\leq M_t \leq N)$ local obstacles to P^1 and the remaining $M^2 = M_t - M^1$ to P^2 . Then the total time taken by HyPRAP in generating predictions only is $M^1 \Delta T^1 + M^2 \Delta T^2$.

The proof of this result follows from elementary calculation given the variables we have defined in Section V-A. More importantly, the result is intuitive. At a time where all three main prediction architectures locally sense the same set of obstacles, we can clearly see that HyPRAP attains better efficiency than SP¹ and worse efficiency than SP²:

$$M_t \Delta T^2 \leq M^1 \Delta T^1 + M^2 \Delta T^2 \leq M_t \Delta T^1 \quad (7)$$

Thus, as P-CRI routes more obstacles from P^1 to P^2 , the computation efficiency of HyPRAP improves, while overall prediction accuracy degrades.

C. Confidence-based Safety Analysis

To simplify notation in our results, we define the following vector of individual prediction errors $\mathbf{e}[t + h]$ and stacked

conformal regions $\epsilon[t + h|t]$.

$$\mathbf{e}[t + h] \triangleq \left[\|Y_k[t + h] - \hat{Y}_k^{\phi(t,k)}[t + h|t]\| \right]_{k=1}^{M_t} \quad (8a)$$

$$\epsilon[t + h|t] \triangleq \left[\epsilon^{\phi(t,k)}[t + h|t] \right]_{k=1}^{M_t} \quad (8b)$$

Lemma 2 (Safety Bounds of HyPRAP). Given (1) holds for a single obstacle k and prediction model P^ℓ at fixed confidence level $1 - \bar{\delta}$, the following bound holds when HyPRAP is predicting for M_t obstacles at time t :

$$\mathbb{P}(\mathbf{e}[t + h] \leq \epsilon[t + h|t]) \geq 1 - M_t \bar{\delta} \quad (9)$$

where $h \in \{1, \dots, H\}$, $\mathbf{e}[t + h]$, $\epsilon[t + h|t]$ are from (8).

Proof. Define the events

$$A_k \triangleq \{ \|Y_k[t + h] - \hat{Y}_k^{\phi(t,k)}[t + h|t]\| \leq \epsilon^{\phi(t,k)}[t + h|t] \}$$

so that $\mathbb{P}(A_k) \geq 1 - \bar{\delta}$, $\forall k \in \{1, \dots, M_t\}$ by (1). By Bonferroni's inequality, we get

$$\mathbb{P}\left(\bigcap_{k=1}^{M_t} A_k\right) \geq 1 - \sum_{k=1}^{M_t} (1 - \mathbb{P}(A_k)) \geq 1 - M_t \bar{\delta}.$$

Since the inequality $\mathbf{e}[t + h] \leq \epsilon^\ell[t + h|t]$ where ϵ^ℓ contains information of prediction model P^ℓ element-wise, holds if and only if A_k holds for all k , the result is proved. \square

Note that the right side of (9) is independent of prediction architecture, which means both single-predictor models and HyPRAP are capable of attaining the same safety guarantee. The key difference is the size of the *conformal region* ϵ with which the bound can be met. Because P^1 has the most accurate bound per obstacle, it can reach the bound at a smaller conformal region compared to P^2 ; the collective conformal regions of HyPRAP fall in between SP^1 and SP^2 . Thus, we observe a similar trend among the three architectures as Lemma 1, but with the order reversed.

Remark 2. The bound derived in Lemma 2 decreases with M_t . Similar to how we defined $\bar{\delta}$ to construct (2), we can offset the decreasing confidence bound by setting $\bar{\delta}$ to be δ/M_t (and to ensure (2), we would set $\bar{\delta} \triangleq \delta/M_t H$). Since M_t changes with time as the agent locally observes its environment, a simpler (but tight and uninformed) choice would be δ/N . A better way is to precompute ϵ^ℓ at each M_t and H offline with the calibration data, then construct an ϵ -table for efficient online lookup.

The next lemmas consider the confidence of HyPRAP under the special case when obstacles are non-interacting, which is a common assumption used in many applications (e.g., self-driving vehicles, robotics) for its simple implementation and reasonable approximation of reality.

Lemma 3 (Safety Bounds Under Non-Interaction). Assume that all obstacles are non-interacting. Given (1) holds for a single obstacle k and prediction model P^ℓ for fixed confidence level $1 - \bar{\delta}$, the following bound holds when HyPRAP is predicting for M_t obstacles at time t :

$$\mathbb{P}(\mathbf{e}[t + h] \leq \epsilon^\ell[t + h|t]) \geq (1 - \bar{\delta})^{M_t} \quad (10)$$

where $h \in \{1, \dots, H\}$, and $\mathbf{e}[t + h]$, $\epsilon[t + h|t]$ are from (8).

The proof follows similarly to that of Lemma 2, but in place of Bonferroni's result, we can simply take the product since the A_k are independent events.

The previous two lemmas were derived assuming obstacles treated by both P^1 and P^2 must satisfy the confidence bound. However, P-CRI typically routes obstacles to less accurate models only if they are less risky to the agent, meaning it is not imperative for all P^2 -routed obstacles to immediately satisfy their respective safety bounds. The following result derives an alternative bound when we add a "partial coverage" relaxation to P^2 .

Lemma 4 (Safety Bounds Under Partial Coverage). Under the same setting as Lemma 3, and events A_k as defined in the proof of Lemma 2, further define indicator random variables $X_k = 1$ if A_k occurs, else 0. Then we have

$$\begin{aligned} & \mathbb{P}\left(\bigcap_{k \in P^1} \{X_k = 1\} \cap \left\{\sum_{k \in P^2} X_k \geq \alpha M^2\right\}\right) \\ & \geq (1 - \bar{\delta})^{M^1} \left(\sum_{j=\lceil \alpha M^2 \rceil} \binom{M^2}{j} (1 - \bar{\delta})^j \bar{\delta}^{M^2-j} \right) \end{aligned} \quad (11)$$

where $h \in \{1, \dots, H\}$, M^2 is the number of obstacles routed to P^2 , and $\alpha \in [0, 1]$ is a *partial coverage* rate.

Proof. Define events $E_1 = \bigcap_{k \in P^1} \{X_k = 1\}$ and $E_2 = \{\sum_{k \in P^2} X_k \geq \alpha M^2\}$. By Lemma 3, we have $\mathbb{P}(E_1) \geq (1 - \bar{\delta})^{M^1}$. Since X_k are Bernoulli and independent, we can use Binomial probabilities to get

$$\mathbb{P}(E_2) \geq \left(\sum_{j=\lceil \alpha M^2 \rceil} \binom{M^2}{j} (1 - \bar{\delta})^j \bar{\delta}^{M^2-j} \right) \geq (1 - \bar{\delta})^{M^2}$$

By assumption, events E_1 and E_2 are independent, thus completing the proof. \square

Remark 3. Lemma 4 enforces that only a certain percentage α of P^2 obstacles must satisfy their confidence bound. Thus, when $\alpha = 1$, it is equivalent to Lemma 3.

Not all predicted obstacle trajectories must be equally accurate for the planner to operate safely as long as the associated risks are appropriately assessed. P-CRI takes advantage of this concept by routing low-risk obstacles to less accurate predictors, instead devoting more computational resources to ensure stricter safety of higher risk obstacles. Even if an obstacle is routed to P^2 , it would not excessively impact the system's safety, since obstacles in P^2 are relatively less risky. Therefore, it is reasonable to consider only a proportion of them using partial coverage. This selective relaxation leads to a tighter overall confidence bound, as shown in (11), compared to the full-coverage case in (10).

Compared to Lemma 2, the non-interacting assumption in Lemmas 3 and 4 generally provides tighter bounds, which is intuitive. Moreover, because P^1 obstacles are more strongly correlated with higher risk than P^2 , Lemma 4 can provide a tighter safety bound than Lemma 3 by adjusting the partial

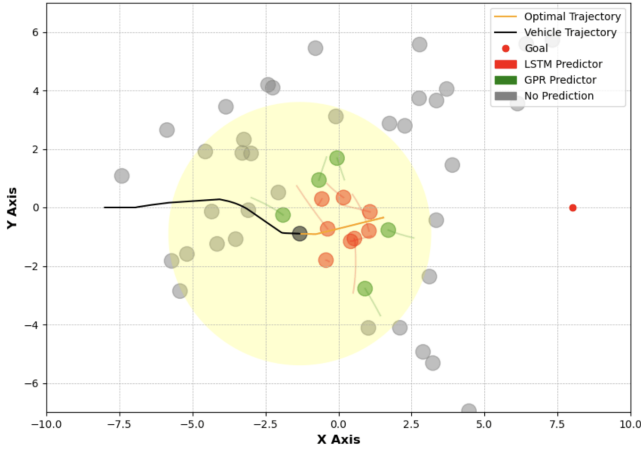


Fig. 3: A sample environment. The agent (black) navigates toward the goal (right red dot) among $N = 50$ obstacles. Here, $N_t = 25$ (yellow shaded) and $M_t = 13$ obstacles are routed to either $P^1 = \text{LSTM}$ (red) or $P^2 = \text{GPR}$ (green); the others remain unpredicted (gray).

coverage parameter α . Deriving a tighter bound in the general case (Lemma 2) is future work.

Remark 4. For simplicity, we presented Section V-C under the assumption of a uniform confidence level across all predictors. However, the overall system confidence can be further improved by allowing a higher failure rate δ for the less accurate predictor P^2 . Deriving HyPRAP’s safety guarantees while allowing each δ to be different for each predictor in \mathcal{P} is future work.

We conclude this section with the emphasis that our theoretical results were derived based on a simplified setting (Section V-A) with the goal of deriving closed-form expressions. In the following Section VI, we remove all of these simplifications, and show empirically that the efficiency and safety trends observed here still hold.

VI. NUMERICAL EXPERIMENTS

To evaluate HyPRAP, we conducted Monte Carlo simulations with 1,000 randomized densely populated scenarios. Each scenario involves anywhere between 20 to 50 obstacles with different motion patterns and initial conditions. The dynamics of our agent follow the kinematic differential drive mobile robot (DDMR) [36]. The MPC problem (3) is posed and solved using CasADi [37] with the IPOPT solver.

Two types of prediction models are utilized: P^1 is a LSTM predictor (high accuracy but lower efficiency) and P^2 is a Gaussian process regression (GPR) predictor (high efficiency but lower accuracy). Both predictors’ conformal regions are calibrated at the same confidence level, $1 - \delta (= 0.95)$. To make sure P-CRI is well-defined, obstacles not assigned to either P^1 or P^2 are predicted with a constant velocity model. We also use hysteresis while routing to avoid frequently switching at a certain threshold. Planning and prediction horizons are both set to $T = H = 30$.

A. Prediction Accuracy-Efficiency Trade-off in HyPRAP

We first follow the structure of Section V and analyze the trade-off between prediction accuracy and com-

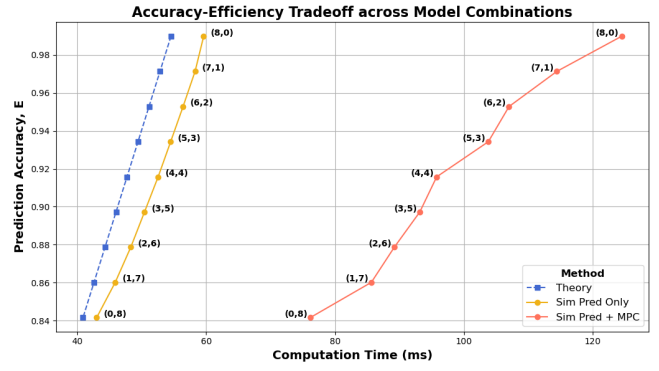


Fig. 4: Prediction accuracy versus computation time under HyPRAP architecture, subject to $M^1 + M^2 = 8$. Each point (M^1, M^2) indicates the case where M^1 obstacles are routed to P^1 (LSTM) and M^2 to P^2 (GPR). “Theory” refers to the formula from (7), where ΔT^ℓ were measured empirically. “Sim” refers to the experimental results averaged over the Monte Carlo trials; “Sim Pred Only” denotes the prediction time only, while “Sim Pred + MPC” includes time for both prediction and MPC-solving.

putational efficiency in Section V-B. We empirically evaluated the efficiency by taking the average computation time across all Monte Carlo trials. Accuracy was evaluated using $E \triangleq \frac{1}{M_t} \{M^1 \exp(-\tilde{\epsilon}^1) + M^2 \exp(-\tilde{\epsilon}^2)\}$ where $\tilde{\epsilon}^\ell \triangleq \frac{1}{H} \sum_{h=1}^H \epsilon^\ell[t + h|t]$ is the average radius of the conformal region for predictor P^ℓ across H . The $\tilde{\epsilon}^\ell$ values in the experiments were 0.01 for LSTM and 0.16 for GPR.

Figure 4 presents results under the HyPRAP architecture, where different predictor allocations are explored. We see that among the variations of HyPRAP, selecting a configuration such that more obstacles are routed to P^1 enhances prediction accuracy, while increasing P^2 allocations helps reduce computational load. This aligns with the theory in Section V-B. Notably, when MPC is included, the total computation time deviates significantly from the linear trend, even if the total number of MPC constraints remains fixed at $M_t = 8$. This is because numerical optimizers like IPOPT allocate more computational effort to active constraints. Since obstacles routed to P^1 are more likely to become active constraints due to their higher risk, the computation time tends to increase as the number of obstacles in P^1 grows.

B. Planning and Navigation Performance

We return to the primary purpose of HyPRAP: ensuring the agent safely reaches its target in as minimum time as possible. We evaluate the overall navigation performance of each architecture from V-A according to three metrics: the *success rate*, *average travel time step*, and *computation time*. The success rate is defined as the percentage of trials in which the agent successfully reaches its goal without any collisions. The average travel time across all successful trials measures how quickly the agent reaches its goal. We also compare their total computation times to evaluate how quickly control inputs are generated under each architecture.

In Table I, we see that the success rate gap between SP^1 and HyPRAP is small, with SP^2 achieving the lowest percentage. First, a lower value of E correlates to a larger conformal region, shrinking the feasible solution space. This increases the likelihood of deadlock (i.e., infeasibility). So,

TABLE I: Comparison of success rate and average travel time step.

Architecture	Success Rate (%)	Avg. Travel Time Step
SP ¹	94.0	181.1±32.4
HyPRAP	93.1	184.9±38.7
SP ²	88.5	231.9±70.4

agents under SP² naturally exhibit lower success rates. Second, SP¹ predicts obstacles using P^1 , leading to the highest E and achieving the best success rate. Finally, HyPRAP leverages two prediction models and effectively assigns P^1 to high-risk obstacles, while using the more efficient P^2 elsewhere. Despite its lower E compared to SP¹, the success rate remains nearly the same, as implied in Section V-C.

SP¹ yields the shortest average travel time, followed closely by HyPRAP, while SP² takes over 25% longer. This is due to the larger conformal radii of P^2 , which shrinks the solution space, leading to less optimal paths. In contrast, HyPRAP and SP¹ mitigate this problem by applying P^1 either selectively or uniformly to high-risk obstacles, thereby expanding the feasible space where it matters most. This allows the planner to find more optimal paths and achieve faster travel times.

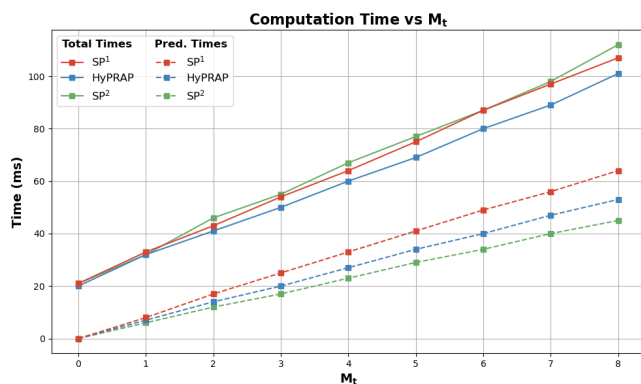


Fig. 5: Average computation times in the setting of Table I. Total times include Prediction and MPC time.

Figure 5 illustrates how the computation time increases over M_t for all three architectures. The order of the architectures in prediction time over M_t matches the analytical result Lemma 1: HyPRAP falls between SP² and SP¹. Comparing Table I and Figure 5, we see the navigation performance benefits of SP¹ come at a higher computational cost than HyPRAP. Whereas SP² attains the lowest navigation quality with the worst total computation time. Therefore, HyPRAP emerges as the most balanced architecture, reducing computational demands while achieving near-optimal performance.

To explain why SP² exhibits the highest computation time in Figure 5, we remark that MPC with a NLP solver employs a warm-start strategy to accelerate convergence. However, during navigation, rapid changes in the environment—such as sharp turns or sudden replanning triggered by newly observed obstacles through local sensing—can render the previous solution inconsistent with the current state. In such cases, the solver must explore a substantially different solution space, and warm-start may hinder convergence or trap

the solver in a local minimum. This problem is exacerbated in SP² due to larger obstacle sizes, which further shrink the feasible region. Note that the total computation time of SP² in Figure 5 differs from that of HyPRAP at (0, 8) in Figure 4. The former accounts for all obstacle configurations under $M_t = 8$, whereas the latter reflects only low-risk obstacles that are routed to P^2 by the P-CRI mechanism. Overall, we see the diminishing solution space not only increases the chance of infeasibility but also impairs the controller’s responsiveness. This leads us to an important design principle when choosing predictors in \mathcal{P} :

Overly conservative or low-quality prediction models can excessively shrink the MPC’s feasible solution space, thereby degrading performance.

C. P-CRI vs. Other Risk Assessment Methods

To highlight the advantages of P-CRI over other metrics, we also perform experiments comparing HyPRAP architectures where the risk metric is varied while the predictors are kept the same. We compare it against a heuristic proximity-based method, which, unlike P-CRI, only uses distance to the obstacle to measure its risks. P-CRI captures more information as described in IV-D. We calibrated the proximity method in two ways. *Prox.A* is calibrated to match P-CRI’s computational load, measured by the average number of prediction model calls (LSTM and GPR) per scenario. *Prox.B* is tuned to achieve a similar success rate to P-CRI.

TABLE II: Comparison of success rate and prediction model calls.

Architecture	Success Rate (%)	Model Calls		
		LSTM	GPR	Total
<i>Prox.A</i>	80.3	361	226	587
<i>Prox.B</i>	93.6	999	591	1590
P-CRI	93.1	422	170	592

Prox.A yields a significantly lower success rate than P-CRI, revealing limitations in using only distance to capture imminent risk. In contrast, *Prox.B* maintains about the same level of safety as P-CRI, but it also calls each predictor 2-3 times more. These results demonstrate that the hybrid distance-time implementation of P-CRI allows HyPRAP to balance safety and computational load, analogous to how the hybrid combination of multiple predictors can achieve the safety-efficiency balance. Moreover, a key limitation of proximity-based methods is their inability to anticipate obstacles that are about to intersect with the agent’s predicted trajectory. Thus, the safety boundaries may be activated too late to respond effectively, making the MPC problem infeasible. In contrast, P-CRI assesses the risk over time, allowing for timely and appropriate predictor allocation.

VII. CONCLUSION

We proposed HyPRAP, a hybrid conformal prediction framework for safe and efficient planning in dense, uncertain environments. The framework uses our novel Prediction-based Collision Risk Index (P-CRI) to dynamically allocate computational effort to high-risk obstacles. We theoretically

demonstrated that HyPRAP achieves the best balance of computational efficiency and safety compared to architectures using single predictors. Numerical experiments validated our theories under far more complex scenarios, demonstrating that HyPRAP achieves better success rates and path qualities than other methods, while reducing computation time. To enhance real-time feasibility in practical prediction-based planning, further research is warranted through algorithmic optimization and hardware acceleration. Future work will also focus on refining P-CRI by estimating the probability of active constraints at the MPC solver level, incorporating interaction-aware predictors, and extending the framework to multi-agent planning.

REFERENCES

- [1] E. Frazzoli, M. A. Dahleh, and E. Feron, "Real-time motion planning for agile autonomous vehicles," *Journal of guidance, control, and dynamics*, vol. 25, no. 1, pp. 116–129, 2002.
- [2] S. Karaman and E. Frazzoli, "Optimal kinodynamic motion planning using incremental sampling-based methods," in *49th IEEE conference on decision and control (CDC)*. IEEE, 2010, pp. 7681–7687.
- [3] G. S. Aoude, B. D. Luders, J. M. Joseph, N. Roy, and J. P. How, "Probabilistically safe motion planning to avoid dynamic obstacles with uncertain motion patterns," *Autonomous Robots*, vol. 35, no. 1, pp. 51–76, 2013.
- [4] A. Mesbah, "Stochastic model predictive control: An overview and perspectives for future research," *IEEE Control Systems Magazine*, vol. 36, no. 6, pp. 30–44, 2016.
- [5] T. Brüdigam, M. Olbrich, D. Wollherr, and M. Leibold, "Stochastic model predictive control with a safety guarantee for automated driving," *IEEE Transactions on Intelligent Vehicles*, vol. 8, no. 1, pp. 22–36, 2023.
- [6] L. Lindemann, M. Cleaveland, G. Shim, and G. J. Pappas, "Safe planning in dynamic environments using conformal prediction," *IEEE Robotics and Automation Letters*, 2023.
- [7] A. Dixit, L. Lindemann, S. X. Wei, M. Cleaveland, G. J. Pappas, and J. W. Burdick, "Adaptive conformal prediction for motion planning among dynamic agents," in *Learning for Dynamics and Control Conference*. PMLR, 2023, pp. 300–314.
- [8] Z. Xie, P. Xin, and P. Dames, "Towards safe navigation through crowded dynamic environments," in *2021 IEEE/RSJ International Conference on Intelligent Robots and Systems (IROS)*. IEEE, 2021, pp. 4934–4940.
- [9] A. Prutsch, H. Bischof, and H. Possegger, "Efficient motion prediction: A lightweight & accurate trajectory prediction model with fast training and inference speed," in *2024 IEEE/RSJ International Conference on Intelligent Robots and Systems (IROS)*, 2024, pp. 9411–9417.
- [10] L. Liu and J. Deng, "Dynamic deep neural networks: optimizing accuracy-efficiency trade-offs by selective execution," in *Proceedings of the 32nd AAAI Conference on Artificial Intelligence*. AAAI Press, 2018.
- [11] Y. Huang and P. Van Gelder, "Collision risk measure for triggering evasive actions of maritime autonomous surface ships," *Safety science*, vol. 127, p. 104708, 2020.
- [12] D. Kahneman, *Thinking, fast and slow*. New York: Farrar, Straus and Giroux, 2011.
- [13] Figure, "Helix: A vision-language-action model for generalist humanoid control," <https://www.figure.ai/news/helix>.
- [14] Y. Nakahira, Q. Liu, T. J. Sejnowski, and J. C. Doyle, "Diversity-enabled sweet spots in layered architectures and speed-accuracy trade-offs in sensorimotor control," *Proceedings of the National Academy of Sciences*, vol. 118, no. 22, p. e1916367118, 2021.
- [15] F. Borrelli, A. Bemporad, and M. Morari, *Predictive control for linear and hybrid systems*. Cambridge University Press, 2017.
- [16] J. B. Rawlings and M. J. Risbeck, "Model predictive control with discrete actuators: Theory and application," *Automatica*, vol. 78, pp. 258–265, 2017.
- [17] A.-T. Tran, A. Muraleedharan, H. Okuda, and T. Suzuki, "Scenario-based stochastic MPC for vehicle speed control considering the interaction with pedestrians," *IFAC-PapersOnLine*, vol. 53, no. 2, pp. 15 325–15 331, 2020, 21st IFAC World Congress.
- [18] L. Hewing, J. Kabzan, and M. N. Zeilinger, "Cautious model predictive control using Gaussian process regression," *IEEE Transactions on Control Systems Technology*, vol. 28, no. 6, pp. 2736–2743, 2020.
- [19] L. Blackmore, M. Ono, and B. C. Williams, "Chance-constrained optimal path planning with obstacles," *IEEE Transactions on Robotics*, vol. 27, no. 6, pp. 1080–1094, 2011.
- [20] J. Lei and L. Wasserman, "Distribution-free prediction bands for non-parametric regression," *Journal of the Royal Statistical Society Series B: Statistical Methodology*, vol. 76, no. 1, pp. 71–96, July 2013.
- [21] R. J. Tibshirani, R. F. Barber, E. J. Candès, and A. Ramdas, "Conformal prediction under covariate shift," in *Proceedings of the 33rd International Conference on Neural Information Processing Systems*. Curran Associates Inc., 2019.
- [22] J. Fisac, A. Bajcsy, S. Herbert, D. Fridovich-Keil, S. Wang, C. Tomlin, and A. Dragan, "Probabilistically safe robot planning with confidence-based human predictions," in *Robotics*, ser. Robotics: Science and Systems. MIT Press Journals, 2018.
- [23] D. Fridovich-Keil, A. Bajcsy, J. F. Fisac, S. L. Herbert, S. Wang, A. D. Dragan, and C. J. Tomlin, "Confidence-aware motion prediction for real-time collision avoidance," *The International Journal of Robotics Research*, vol. 39, no. 2-3, pp. 250–265, 2020.
- [24] C. G. Prevost, A. Desbiens, and E. Gagnon, "Extended Kalman filter for state estimation and trajectory prediction of a moving object detected by an unmanned aerial vehicle," in *2007 American Control Conference*, 2007, pp. 1805–1810.
- [25] A. Elnagar, "Prediction of moving objects in dynamic environments using Kalman filters," in *Proceedings 2001 IEEE International Symposium on Computational Intelligence in Robotics and Automation*, 2001, pp. 414–419.
- [26] N. Morales, J. Toledo, L. Acosta, and J. Sánchez-Medina, "A combined voxel and particle filter-based approach for fast obstacle detection and tracking in automotive applications," *IEEE Transactions on Intelligent Transportation Systems*, vol. 18, no. 7, pp. 1824–1834, 2017.
- [27] D. Schulz, W. Burgard, D. Fox, and A. Cremers, "Tracking multiple moving targets with a mobile robot using particle filters and statistical data association," in *Proceedings 2001 ICRA. IEEE International Conference on Robotics and Automation (Cat. No.01CH37164)*, vol. 2, 2001, pp. 1665–1670 vol.2.
- [28] A. Vakanski, I. Mantegh, A. Irish, and F. Janabi-Sharifi, "Trajectory learning for robot programming by demonstration using hidden Markov model and dynamic time warping," *IEEE Transactions on Systems, Man, and Cybernetics, Part B (Cybernetics)*, vol. 42, no. 4, pp. 1039–1052, 2012.
- [29] D. Vasquez, T. Fraichard, and C. Laugier, "Incremental learning of statistical motion patterns with growing hidden Markov models," *IEEE Transactions on Intelligent Transportation Systems*, vol. 10, no. 3, pp. 403–416, 2009.
- [30] S. Hochreiter and J. Schmidhuber, "Long short-term memory," *Neural computation*, vol. 9, no. 8, pp. 1735–1780, 1997.
- [31] A. Alahi, K. Goel, V. Ramanathan, A. Robicquet, L. Fei-Fei, and S. Savarese, "Social LSTM: Human trajectory prediction in crowded spaces," in *Proceedings of the IEEE conference on computer vision and pattern recognition*, 2016, pp. 961–971.
- [32] K. Kim, D. Lee, and I. Essa, "Gaussian process regression flow for analysis of motion trajectories," in *2011 International Conference on Computer Vision*. IEEE, 2011, pp. 1164–1171.
- [33] L. Zhao and X. Fu, "A method for correcting the closest point of approach index during vessel encounters based on dimension data from ais," *IEEE Transactions on Intelligent Transportation Systems*, vol. 23, no. 8, pp. 13 745–13 757, 2022.
- [34] M. Radanovic, M. A. Piera Eroles, T. Koca, and J. J. Ramos Gonzalez, "Surrounding traffic complexity analysis for efficient and stable conflict resolution," in *Transportation Research Part C: Emerging Technologies*, vol. 95. Elsevier, 2018, pp. 105–124.
- [35] A. S. Lenart, "Analysis of collision threat parameters and criteria," *The Journal of Navigation*, vol. 68, no. 5, pp. 887–896, 2015.
- [36] R. Siegwart, I. R. Nourbakhsh, and D. Scaramuzza, *Introduction to autonomous mobile robots*. MIT press, 2011.
- [37] J. A. E. Andersson, J. Gillis, G. Horn, J. B. Rawlings, and M. Diehl, "CasADi – A software framework for nonlinear optimization and optimal control," *Mathematical Programming Computation*, vol. 11, no. 1, pp. 1–36, 2019.